3.4 IRRADIATION CREEP OF NEAR-STOICHIOMETRIC SILICON CARBIDE FIBERS — T. Koyanagi, K. Ozawa (Oak Ridge National Laboratory), T. Hinoki (Kyoto University), L.L. Snead, Y. Katoh (Oak Ridge National Laboratory)

OBJECTIVE

The objective of this work is to evaluate the irradiation creep behavior of near-stoichiometric silicon carbide (SiC) fibers to aid in the understanding of the performance of SiC composite as fusion reactor structural components.

SUMMARY

The neutron irradiation creep of near-stoichiometric SiC fibers was evaluated by bend stress relaxation (BSR) tests. The results indicate that the apparent stress exponent of the irradiation creep of the SiC fibers is near unity at ~500°C. The instantaneous creep compliance of the SiC fibers, which is the creep strain normalized to the applied stress and neutron flux, was estimated to be ~1×10^{-7} [MPa^{-1} dpa^{-1}] at ~6 dpa. The creep compliance values are orders of magnitude smaller than previously reported from light ion irradiation experiments [1]. Quality of the fibers slightly affected the creep behavior: Hi-Nicalon™ Type S fiber showed more creep than other fibers, including Tyranno™ SA3, isotopically-controlled Sylramic™ and Sylramic™ iBN fibers at ~500°C to ~1 dpa.

PROGRESS AND STATUS

Introduction

The service life of ceramic matrix composites (CMC) is often governed by a slow crack growth phenomenon [2]. For continuous SiC fiber reinforced CMC in high radiation operating environments, the slow crack growth is expected to be governed by irradiation creep of bridging fibers and environmentally-induced recession of exposed interphase. Recently, the irradiation creep of high-purity CVD SiC was shown to operate very slowly compared to metals [3]. The underlying mechanism for the primary transient irradiation creep was reported to be swelling-coupled creep caused by anisotropic evolutions of the multi-dimensional defect clusters under applied stresses [3]. However, the irradiation creep of SiC fibers is only poorly understood. The neutron-irradiation creep has not been reported, though a few papers report data on the creep behavior under ion and proton irradiations [4-6]. This report presents data concerning the evaluation of the creep behavior of near-stoichiometric SiC fibers under neutron irradiation.

To evaluate the irradiation creep strain, the BSR test was used. This is one of bend type test techniques, which can evaluate creep properties of ceramic fibers [7]. The BSR method is useful for neutron irradiation experiments because it enables the application of stress to miniature specimens under irradiation, and it requires only very simple post-irradiation measurement. The quantitative evaluation and mechanistic study of irradiation creep of monolithic SiC materials has been reported using this method [3, 8]. However, there are limitations for this test: Applied stress is not constant and uniform in sample during the experiment. The applied stress approaches zero during testing. Therefore, the determination of the creep is impossible after the initial stress is fully relaxed. The non-uniform stress state in test specimens makes the analysis difficult in a certain case. All the data concerning creep rate and stress exponent (*n*) of creep can be obtained from BSR test if the specimen exhibits a uniform isotropic microstructure and creep behavior linear with stress. Because the experimental results showed that the creep behavior of the fibers appeared linear to the applied stress, the quantitative analysis of the irradiation creep was conducted in this study, assuming that the microstructures of the fibers are uniform. Microstructural analyses on the near-stoichiometric SiC fibers were reported by Dong et al. and Sauder et al. [9, 10]. Based on their results, microstructure of Hi-Nicalon™ Type S fiber is uniform. On the other hand, the uniformity of microstructure in Tyranno™ SA fibers depends on the batch. Slyramic™ fiber has a slightly different microstructure between near the fiber edge at the core.

Experimental Procedure

Materials

The materials used in this work were Hi-Nicalon™ Type S (Nippon Carbon Co., Tokyo, Japan, lot number: 407203 March 2005), Tyranno™ SA3 (Ube Industry Ltd., Tokyo, Japan, type: S1I16PX, lot number: 4303), experimental-grade Sylramic™ (COI Ceramics, Inc., California, USA, lot number: 4240, spool 01A), and experimental-grade Sylramic™ iBN (COI Ceramics, Inc., California, USA, lot number: 4630, spool 01B) SiC-based fibers. The key properties of these fibers are presented in

Table **1**. The properties other than grain size were obtained from material data sheet provided from the venders. Information of the grain size can be found elsewhere [10, 11]. Note that the Sylramic™ and Sylramic™ iBN fibers in this work are isotopically-controlled, which mainly contain ^{11}B instead of ^{10}B. The properties of these two fibers are assumed to be same as those of commercial ones except for the type of the isotope.

Table 1. Properties of near-stoichiometric SiC fibers.

Materials	**Elemental Composition [wt.%]**	**Carbon Impurity [wt.%]**	**Average Diameter [μm]**	**Young's Modulus [Gpa]**	**Grain Size [nm]**
Tyranno™-SA3	67 Si + 31 C + <1 O + <2 Al	2.3	7.5	380	200
Hi-Nicalon™ Type S	69 Si + 31 C + 0.2 O	1.4	12	420	50
Experimental Sylramic™	67 Si + 29 C + 0.8 O + 2.3 ^{11}B + 0.4 N + 2.1 Ti	0.3	10	372	100
Experimental Sylramic™-iBN	67 Si + 29 C + 0.8 O + 2.3 ^{11}B + 0.4 N + 2.1 Ti	0.3	10	372	>100

BSR test

The fiber bundles were attached to a fixture with three different curvature radiuses of 2, 3, and 6 mm to apply flexural stress, and then were irradiated as shown in

Figure 1. The fixture was fabricated from near-stoichiometric graphite to avoid chemical reaction between the fibers and the fixture. The initial bending stress levels systematically ranged from ~200 to ~1400 MPa. Relaxation creep was evaluated using the BSR ratio (*m*), which is the ratio of final stress (σ_a) to initial stress (σ_0). The BSR ratio can be expressed as Eq. (1), where *E*, *ε*, and *R* are the elastic modulus, flexural strain, and curvature radius of the specimen, respectively.

$$m = \frac{\sigma_a}{\sigma_0} = \frac{E_a(\varepsilon_0 - \varepsilon_c)}{E_0\varepsilon_0} = \frac{E_a}{E_0}(1 - \frac{R_a}{R_0}) \qquad (1)$$

The subscripts *a*, *0*, and *c* stand for the initial state, final state, and creep, respectively. The BSR ratio varies between 0 and 1, where 0 indicates complete relaxation and 1 indicates no relaxation. The effect of irradiation on the Young's modulus is assumed to be same as that for CVD SiC [12]. The BSR ratio was evaluated by measuring the curvature radius of the specimen. The curvature radiuses before and after irradiation were obtained using analysis of the images of an individual fiber. The imaging was conducted using KEYENCE, VHX-1000 optical microscope. The creep strain was obtained from the BSR ratio and initial flexural strain according to Eq. (1). Details about the BSR testing procedure can be found elsewhere [7].

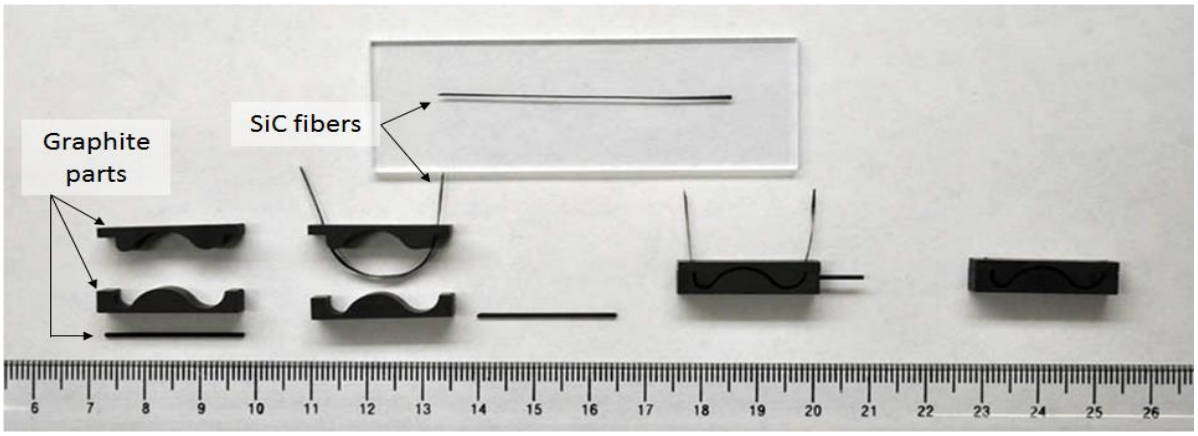

Figure 1. Appearance of the BSR test fixture and SiC fiber specimens.

Neutron irradiation

Neutron irradiation was in the High-Flux Isotope Reactor (HFIR). The specimens were irradiated at 480–1180°C to 0.97–11.87 dpa for SiC (0.97–11.87 × 10^{25} n/m^2, E > 0.1 MeV; and the conversion 1.0 × 10^{25} n/m^2 = 1 dpa is used). The damage rate was ~1.1 × 10^{-6} dpa/s. Experiments to determine the irradiation creep were conducted in an inert-gas atmosphere. The irradiation temperature was determined by dimensional changes on annealing of CVD SiC parts irradiated with the BSR fixture, using a dilatometer. As the SiC parts were designed to be in direct contact with the BSR fixture during irradiation, this measurement represents an accurate sample temperature during irradiation.

Results

Figure 2 shows appearance of the SiC fiber bundles after irradiation at ~500°C to ~1 dpa. The fibers are constrained by the graphite fixture in unirradiated condition as shown in
Figure 1, and the constraint is removed after irradiation as shown in Figure 2. The presence of irradiation creep was clearly observed for all kinds of the fibers at this condition due to the curved appearance. If the irradiation creep was absent, the fibers remained straight as observed in unirradiated condition. The irradiation creep also existed under the other irradiation conditions at ~500°C to ~10 dpa, and at ~1200°C to ~1 dpa.

Stress dependence of the BSR ratios measured in this work is shown in Figure 3. The horizontal error bars indicate the range of flexural stress during irradiation with the highest at the beginning of irradiation and the lowest at the end of irradiation. The vertical error bar is due to the measurement scatter of the pre-irradiation curvatures. Relationship between the stress dependence and the stress exponent (*n*) of the irradiation creep is also presented. The stress exponent is unity if the BSR ratio is independent on applied stress. When the stress exponent is over 1, the BSR ratio decreases with increasing the applied stress. The stress dependence becomes marked with increasing the stress exponent as shown in Figure 3 (e). The stress dependences of the BSR ratio appeared to be insignificant at ~500°C, indicating the apparent stress exponents of the irradiation creep were near unity for the SiC fibers. At ~1200°C, the BSR ratios of Hi-Nicalon^{TM} Type S fiber were independent on applied stress level. However, the stress dependence can exist for the other fibers. The stress dependence of the BSR ratio at ~1200°C will be discussed with additional data points with the neutron fluence of ~10 dpa.

The BSR ratios ranged over approximately 0.3–0.6 under irradiation at 500 and 1200°C to 1 dpa, and 0–0.2 at 500°C to 10 dpa for all fibers. Note that the BSR ratios were similar following irradiation at 500°C to 1 dpa and at 1200°C to 1 dpa, though the temperature was significantly different. Since the contribution of thermal creep to irradiation creep increases at higher temperature, the irradiation-induced creep appeared to be more significant at 500°C.

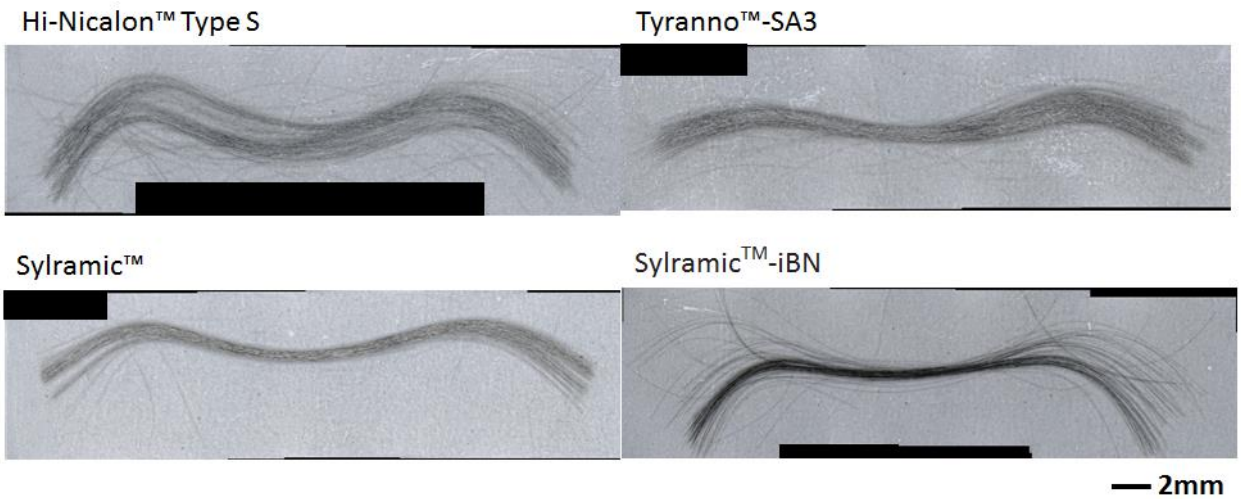

Figure 2. Optical micrographs of SiC fibers following irradiation at ~500°C to ~1 dpa

Table 2. Results of the BSR experiments. Standard deviations in parentheses. Irradiation temperatures determined by dimensional change during annealing of CVD SiC irradiated with the SiC fibers.

Materials	**Irradiation Temperature [°C]**	**Fluence [dpa]**	**Rabbit Capsule ID**	**Number of Measured Curvature**	**Average BSR ratio**
Tyranno™-SA3	560	0.97	TTN16	15	0.59 (0.04)
HI-Nicalon™ Type S	560	0.97	TTN16	24	0.35 (0.06)
Developmental Sylramic™	560	0.97	TTN16	23	0.55 (0.09)
Developmental Sylramic™-iBN	560	0.97	TTN16	24	0.51 (0.06)
Tyranno™-SA3	500	11.87	TTN17	0	
HI-Nicalon™ Type S	500	11.87	TTN17	11	0.08 (0.06)
Developmental Sylramic™	500	11.87	TTN17	11	0.10 (0.07)
Developmental Sylramic™-iBN	500	11.87	TTN17	13	0.11 (0.06)
Tyranno™-SA3	1110	0.97	TTN19	8	0.51 (0.09)
HI-Nicalon™ Type S	1110	0.97	TTN19	11	0.46 (0.04)
Developmental Sylramic™	1110	0.97	TTN19	10	0.61 (0.09)
Developmental Sylramic™-iBN	1110	0.97	TTN19	11	0.56 (0.08)

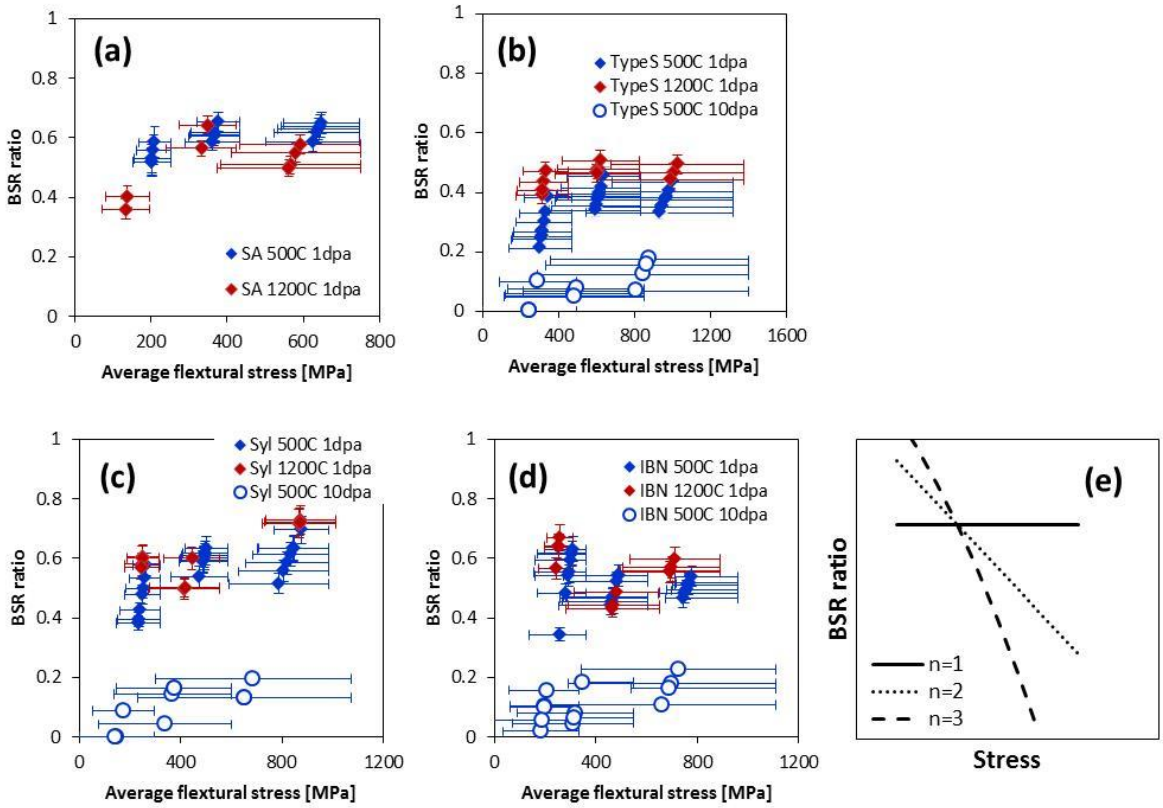

Figure 3. Effect of stress magnitude on BSR ratio in Tyranno™-SA3 (a), Hi-Nicalon™ Type S (b), experimental Sylramic™ (c), and experimental Sylramic™-iBN (d) during neutron irradiation. The horizontal error bars indicate the range of flexural stress during irradiation with the highest at the beginning of irradiation and the lowest at the end of irradiation. The relationship between the stress dependence and the stress exponent (*n*) is also presented (e).

Irradiation fluence dependences of the BSR ratios of the SiC fibers are shown in Figure 4. The graph also contains the data plots of CVD SiC materials including Rohm & Hass polycrystalline 3C SiC having columnar grains with ~1 μm of the column width and with a moderate amount of stacking fault and, CoorsTek polycrystalline 3C SiC having highly faulted columnar grains with ~10 μm of the column width, and Cree 4H single crystal SiC [3]. The data points for the CVD SiC at ~10 dpa have not been published. At ~500°C, the BSR ratios of both the SiC fibers and CVD SiC decreased with increasing fluence, meaning that the irradiation creep occurred till 10 dpa. The BSR ratios of the fibers were clearly smaller than those of CVD SiC ceramics, i.e. the fibers crept more than the CVD SiC materials. Effects of the material quality of the SiC fibers on the BSR ratio was observed at ~500°C to ~1dpa: the Hi-Nicalon™ Type S SiC fiber crept more than the other fibers. On the other hand, the material quality did not affect the creep behavior of CVD SiC, though the poly-type, grain size (the order of micron), and density of the pre-existing stacking fault were different. Since the fibers had different grain-size (the order of nano) and impurities as shown in Table 1, these differences potentially caused the differential creep of the fibers.

In case of the creep at ~1200°C, the BSR ratio was similar among the fibers, considering the error bars. The stress relaxation of the fibers was similar level to polycrystalline CVD SiC provided by Rohm and Haas Company. In contrast to the SiC fiber, differential creep behavior of the CVD SiC materials has been

reported, and is considered to be caused by different degree of the grain-boundary sliding and the basal slip among the materials [3]. At this temperature, the thermal creep of the SiC fibers can have non-negligible contribution to the irradiation creep [11,13].

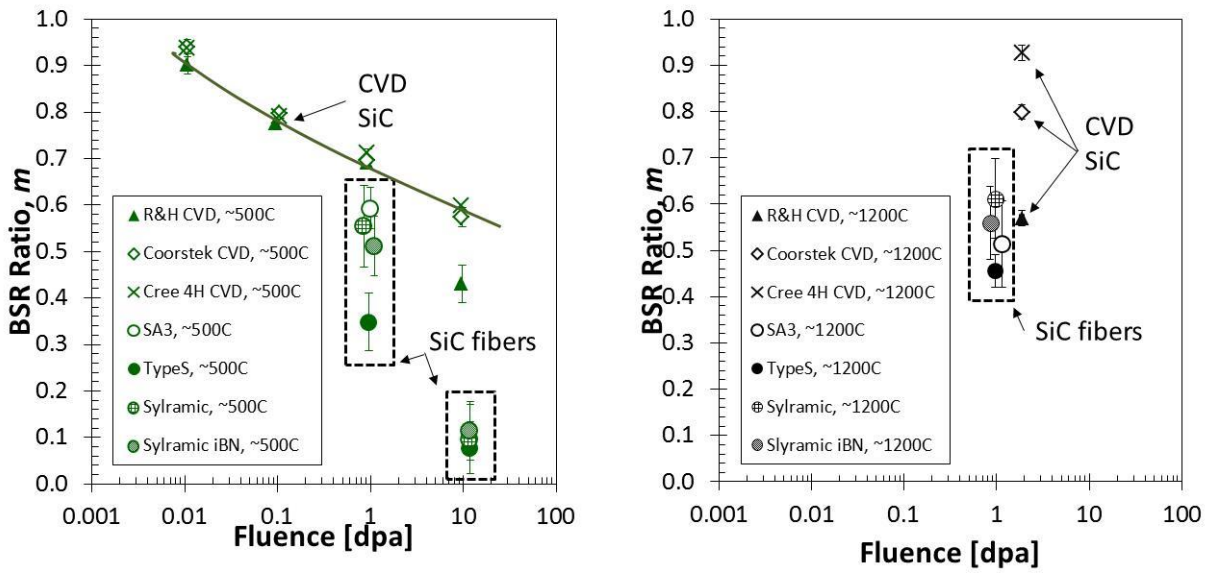

Figure 4. The effect of neutron fluence on the BSR ratio of the SiC fibers. Error bars indicate one standard deviation. The data plots of the fibers were laterally-shifted for visual purpose. The data of CVD SiC is also plotted.

Creep coefficient, which is normalized creep strain with respect to the stress and the neutron fluence is used to compare creep behavior of different materials at low fluence level [14]. The instantaneous creep coefficient (*K*) is defined by:

$$K \cong \frac{\varepsilon_2 - \varepsilon_1}{\sigma(\gamma_2 - \gamma_1)} \qquad (2)$$

where γ_1 and γ_2 ($\gamma_1 < \gamma_2$) are neutron fluences, σ is average stress during irradiation, and ε_1 and ε_2 are irradiation creep strains following irradiation at a fluence of γ_1 and γ_2, respectively. Figure 5 shows the fluence dependence of the instantaneous creep coefficient of the SiC fibers. The highest and lowest error bars indicate the fluence of γ_1 and γ_2 for each data point, respectively. The instantaneous creep coefficient of Tyranno™ SA3 is absent in the figure due to the luck of the creep data. That is expected to be a comparable to those of the experimental-grade Sylramic™ and Sylramic™ iBN fibers based on the similar creep behavior among them in Figure 4. The figure also shows the instantaneous creep coefficient of Rohm & Hass CVD SiC, and the swelling-coupled creep model of CVD SiC at ~300–~500°C [3]. The creep coefficients of the SiC fiber have values of ~1×10^{-7} [MPa^{-1} dpa^{-1}] at ~6 dpa, which is within one order of magnitude of that of CVD SiC. In other words, creep behavior was not dramatically different between the CVD SiC and the SiC fibers, though the SiC fibers crept more than the CVD SiC as shown in Figure 4. Note that the creep coefficient was very small comparing to those of stainless steels (in the order of ~1×10^{-6} [MPa^{-1} dpa^{-1}]) [14]. The swelling-creep coupled model can explain the creep behavior of CVD SiC at the initial transient region (up to ~1 dpa) [3], but cannot explain the creep after the transient. This result indicates the existence of a differential creep mechanism, such as steady state creep. The instantaneous creep coefficient for the steady state creep of the CVD SiC would be ~1×10^{-7} [MPa^{-1} dpa^{-1}], if it exists. A similar steady state creep rate is expected for the SiC fibers.

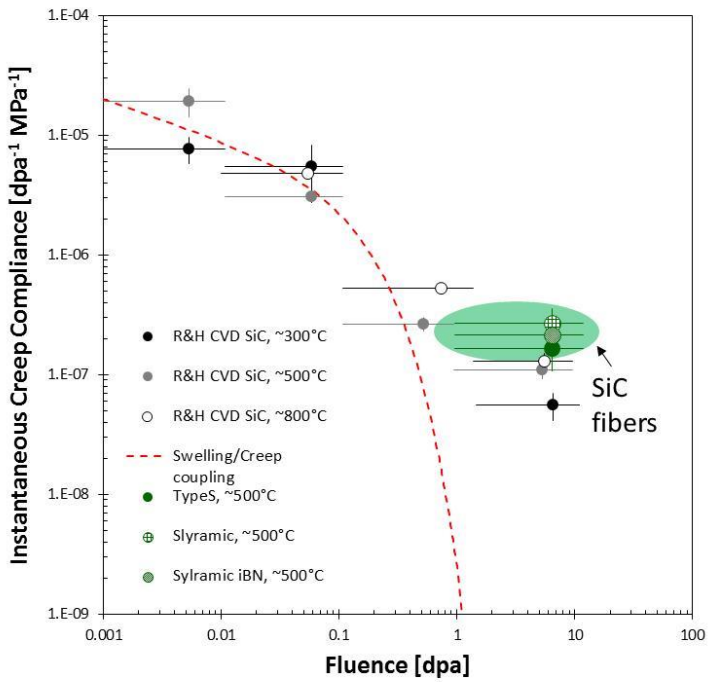

Figure 5. Neutron fluence dependence of instantaneous creep coefficients of SiC fibers. The data for CVD SiC, and the creep coefficients for swelling-coupled creep are included.

References

[1] R. Scholz, G.E. Youngblood, J. Nucl. Mater., 283 (2000) 372.
[2] S. Zhu, M. Mizuno, Y. Kagawa, Y. Mutoh, Composites Science and Technology, 59 (1999) 833.
[3] Y. Katoh, L.L. Snead, C.M. Parish, T. Hinoki, J. Nucl. Mater., 434 (2013) 141.
[4] J. Huguet-Garcia, A. Jankowiak, S. Miro, Y. Serruys, J.M. Costantini, Nuclear Instruments and Methods in Physics Research B, 327 (2014) 93.
[5] R. Scholz, J. Nucl. Mater., 258 (1998) 1533.
[6] R. Scholz, G.E. Youngblood, J. Nucl. Mater., 283 (2000) 372.
[7] G.N. Morscher, J.A. Dicarlo, J. Am. Ceram. Soc., 75 (1992) 136.
[8] T. Koyanagi, K. Shimoda, S. Kondo, T. Hinoki, K. Ozawa, Y. Katoh, J. Nucl. Mater., 455 (2014) 73.
[9] S.M. Dong, G. Chollon, C. Labrugère, M. Lahaye, A. Guette, J.L. Bruneel, M. Couzi, R. Naslain, D.L. Jiang, J. Mater. Sci., 36 (2001) 2371.
[10] C. Saude, J. Lamon, J. Am. Ceram. Soc., 90 (2007) 1146.
[11] J.A. DiCarlo, H.-M. Yun, (2005), Non-oxide (Silicon Carbide) Fibers, Handbook of Ceramic Composites, N. P. Bansal, Ed., Springer Science+Business Media, Inc., 33–52.
[12] L.L. Snead, T. Nozawa, Y. Katoh, T.-S. Byun, S. Kondo, D.A. Petti, J. Nucl. Mater., 371 (2007) 329.
[13] J.J. Sha, J.S. Park, T. Hinoki, A. Kohyama, Mechanics of Materials 39 (2007) 175.
[14] K. Ehrlich, J. Nucl. Mater. 100 (1981) 149.